

# TGBFormer: Transformer-GraphFormer Blender Network for Video Object Detection

Qiang Qi, Xiao Wang\*

School of Data Science, Qingdao University of Science and Technology, Qingdao, China  
qiangq@qust.edu.cn, xiaowang@qust.edu.cn

## Abstract

Video object detection has made significant progress in recent years thanks to convolutional neural networks (CNNs) and vision transformers (ViTs). Typically, CNNs excel at capturing local features but struggle to model global representations. Conversely, ViTs are adept at capturing long-range global features but face challenges in representing local feature details. Off-the-shelf video object detection methods solely rely on CNNs or ViTs to conduct feature aggregation, which hampers their capability to simultaneously leverage global and local information, thereby resulting in limited detection performance. In this paper, we propose a Transformer-GraphFormer Blender Network (TGBFormer) for video object detection, with three key technical improvements to fully exploit the advantages of transformers and graph convolutional networks while compensating for their limitations. First, we develop a spatial-temporal transformer module to aggregate global contextual information, constituting global representations with long-range feature dependencies. Second, we introduce a spatial-temporal GraphFormer module that utilizes local spatial and temporal relationships to aggregate features, generating new local representations that are complementary to the transformer outputs. Third, we design a global-local feature blender module to adaptively couple transformer-based global representations and GraphFormer-based local representations. Extensive experiments demonstrate that our TGBFormer establishes new state-of-the-art results on the ImageNet VID dataset. Particularly, our TGBFormer achieves 86.5% mAP while running at around 41.0 FPS on a single Tesla A100 GPU.

## Introduction

Video object detection aims to predict the location boxes and category labels for each object in videos. It plays an important role in a broad range of applications, such as safe driving (He et al. 2024; Chitta et al. 2023), security surveillance (Li et al. 2019; Zhang et al. 2022) and activity understanding (Liu, Wu, and Jia 2016; Liu et al. 2020). In the past decades, image object detection has achieved immense progress and delivered significant improvement in performance. Unfortunately, these well-built image object detectors suffer from remarkable performance drop when applied to video data,

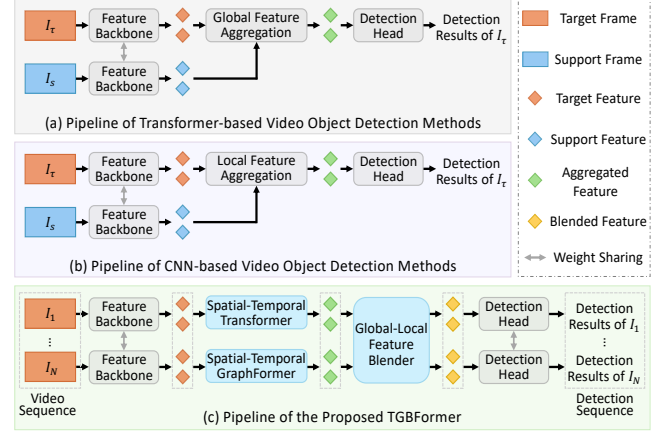


Figure 1: Pipeline comparison of different methods.

due to the appearance deterioration situations arising from motion blur, partial occlusion and unusual poses.

Since videos come with extra temporal information compared to static images, it is intuitive to make full use of the temporal information to alleviate the appearance deterioration situations. Based on this intuition, some off-the-shelf video object detection methods (Qianyu et al. 2023; Deng, Chen, and Wu 2023; Wang et al. 2022; An et al. 2024), whose pipeline is illustrated in Figure 1(a), put efforts into leveraging the long-range temporal dependencies captured by different types of vision transformers to aggregate features from a global perspective. Typically, vision transformers are adept at capturing long-range global information but face challenges in representing short-range local information (Peng et al. 2023; Chen et al. 2023; Yoo et al. 2023). Thus, these transformer-based video object detection methods do not fully consider short-range temporal dependencies and thus lack the local perception capability for objects, which possibly leads to the false detection problem. Some other existing video object detection methods (Qi et al. 2023a; He et al. 2022b; Jiang et al. 2019; Qi, Yan, and Wang 2024), whose pipeline is shown in Figure 1(b), devote to exploiting the short-range temporal dependencies provided by different types of convolutional neural networks (CNNs) to aggregate features from a local perspective. However, CNNs

\*Corresponding Author.

Copyright © 2025, Association for the Advancement of Artificial Intelligence (www.aaai.org). All rights reserved.

are observed to excel at modeling short-range local information but struggle to capture long-range global information (Chen et al. 2023; Yoo et al. 2023). Thus, these CNN-based video object detection methods do not take long-range temporal dependencies into consideration and thus lack the global perception capability for objects, which may result in the missed detection problem. In contrast, the human visual system can simultaneously leverage long-range and short-range temporal information to achieve more comprehensive perception capability for objects. Such a fact motivates us to combine the advantages of transformers and CNNs to improve the video object detection task, which has not been investigated in previous video object detection works.

In this paper, we propose a Transformer-GraphFormer Blender Network (TGBFormer) for video object detection, whose pipeline is illustrated in Figure 1(c), including three key technical improvements to sufficiently combine the advantages of transformers and graph convolutional networks while compensating for their limitations. Although it is easy to think of combining the transformer and GraphFormer models, a simple ensemble of these two models is costly and yields marginal performance improvements. To achieve an effective and efficient combination of them, there are three crucial problems that need to be addressed: i) how to customize the transformer and GraphFormer to aggregate beneficial information, constituting the global and local representations of objects; ii) how to couple the transformer global representations and GraphFormer local representations in a complementary and interactive paradigm, retaining the global modeling capability of transformers and local modeling capability of CNNs to the maximum extent; iii) how to improve inference/running speed, striking a balance between detection accuracy and inference speed. To address the first problem, we develop a spatial-temporal transformer module that exploits long-range spatial and temporal dependencies to aggregate beneficial features, constituting the global representations of objects. Moreover, we present a spatial-temporal GraphFormer module that utilizes short-range spatial and temporal relationships to aggregate useful features, generating new local representations that are complementary to the transformer outputs. To handle the second problem, we design a global-local feature blender module to adaptively couple the transformer global representations and GraphFormer local representations, retaining the global perception capability of transformers and local modeling capability of CNNs to the maximum extent. To solve the third problem, contrary to the non-parallel frame-wise detection fashion that is commonly used in previous video object detection works, we adopt a parallel sequence-wise detection fashion in view of the advantage of TGBFormer’s comprehensive (including both global and local) object perception capability, which simultaneously detects objects on all input frames and thus significantly improves inference speed.

The above customized components are closely integrated into a uniform framework, allowing our TGBFormer to effectively combine the strengths of transformers and graph convolutional networks to produce more comprehensive appearance representations, which facilitates improving video object detection performance. To the best of our knowledge,

our TGBFormer is the first effort that exploits the complementarity of transformer global information and CNN local information to tackle the video object detection task.

We summarize the key contributions as follows:

- We propose a novel Transformer-GraphFormer Blender Network (TGBFormer) for video object detection, which combines the merits of transformers and graph convolutional networks while compensating for their limitations, thereby establishing new state-of-the-art results on the ImageNet VID dataset.
- We introduce two collaborative modules, termed spatial-temporal transformer and GraphFormer modules, that use global and local spatial-temporal dependencies to aggregate features respectively, enabling our TGBFormer to harness the capability of transformers to capture global information while embracing the power of graph convolutional networks to model local information.
- We design a global-local feature blender module to fuse transformer-style global features and GraphFormer-style local features in a complementary fashion, making our TGBFormer preserve the global and local perception capabilities for objects to the maximum extent.

## Related Work

Research on video object detection has proceeded along two directions: CNN-based video object detection methods and transformer-based video object detection methods.

CNN-based video object detection methods (Qi et al. 2023a; He et al. 2022b; Jiang et al. 2019; Qi, Yan, and Wang 2024) usually put efforts into leveraging the temporal dependencies captured by different types of convolutional neural networks (CNNs) or operations to aggregate beneficial features. Typically, CNNs excel at capturing short-range information but face challenges in modeling long-range information (Chen et al. 2023; Peng et al. 2023; Yoo et al. 2023). Thus, these CNN-based video object detection methods fail to fully exploit long-range temporal dependencies, which limits their global perception capability for objects.

Transformer-based video object detection methods (Qianyu et al. 2023; Wang et al. 2022; Cui 2023; An et al. 2024) generally put efforts into leveraging the long-range temporal dependencies captured by different types of vision transformers to aggregate beneficial features. However, transformers are observed to excel at modeling long-range information but struggle to capture short-range information (Peng et al. 2023; Chen et al. 2023; Yoo et al. 2023). Thus, these transformer-based video object detection methods do not fully exploit short-range temporal dependencies, limiting their local perception capability for objects.

Different from these methods that solely rely on CNNs or transformers to model temporal information, our TGBFormer customizes CNNs and transformers in a unified video object detection framework, and combines the merits of both CNNs and transformers to simultaneously explore short-range and long-range temporal information.

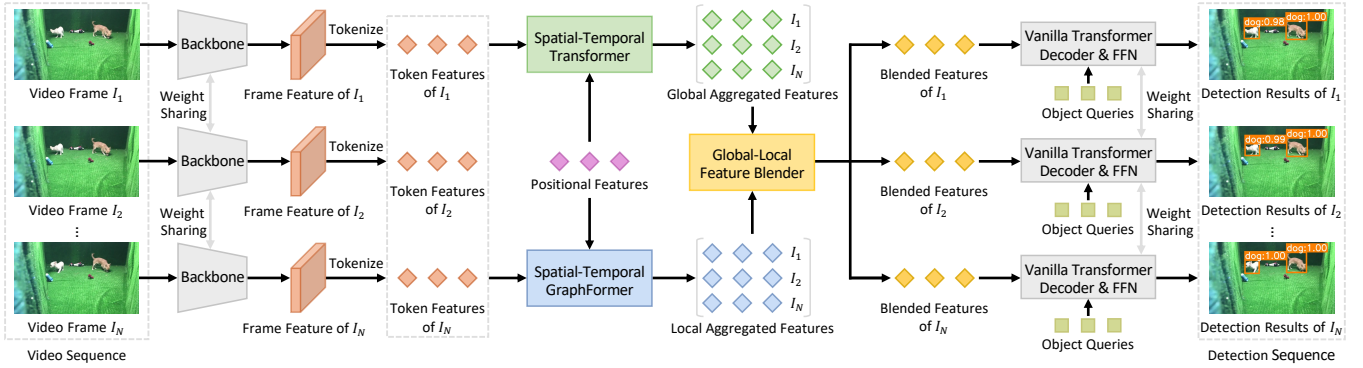


Figure 2: Framework of the proposed TGBFormer, which builds upon the DETR (Carion et al. 2020) model.

## The Proposed Method

### TGBFormer Framework

Figure 2 illustrates the framework of our TGBFormer, which mainly includes three elaborately-customized modules to sufficiently exploit the merits of transformers and graph convolutional networks while compensating for their limitations. Given an input video sequence, each video frame is first processed by a shared backbone network (e.g., ResNet-101) to generate the frame features, followed by a tokenization operation to produce the token features. Then, these token features together with the corresponding positional features (predicted by DETR (Carion et al. 2020)) are fed into a spatial-temporal transformer module (STTM) to generate the global aggregated features. The carefully-customized STTM utilizes the spatial and temporal transformers to explore long-range spatial-temporal dependencies and aggregate beneficial features, enabling our TGBFormer to embrace the global perception capability for objects. Meanwhile, a spatial-temporal GraphFormer module (STGM) is developed to explore short-range spatial-temporal dependencies and aggregate useful features by using the spatial and temporal dynamic graph convolutional networks, generating the local aggregated features that are complementary to the outputs of STTM and thus making our TGBFormer have the local perception capability for objects. After that, a global-local feature blender module is designed to couple the global and local aggregated features in a complementary and interactive fashion, outputting the blended features. Finally, the blended features together with the object queries (generated by DETR) are fed into a vanilla transformer decoder and feed forward network (FFN) to predict detection results. In view of the advantages of our elaborately-customized modules, a parallel sequence-wise detection fashion is adopted in the framework, allowing to simultaneously detect objects on all input frames and thus endowing our TGBFormer with real-time inference speed.

### Spatial-Temporal Transformer Module

The illustration of the proposed STTM is presented in Figure 3. Given the frame feature  $f_n \in \mathbb{R}^{c \times h \times w}$  of the  $n$ -th frame extracted by the backbone network, in which  $c$ ,  $h$  and  $w$  respectively denote the dimension, height and width of

the frame feature, we first tokenize it into non-overlapping  $M (= h \times w)$  token features with the dimension of  $D$ . Then, the token features and the corresponding positional features (generated by DETR (Carion et al. 2020)) of each frame are added together and fed into a spatial multi-head self-attention block to effectively explore long-range spatial dependencies within a frame and perform intra-frame feature aggregation from a global perspective. Building on the success of (Zhu et al. 2021), the calculation of the spatial multi-head self-attention (SpatMHSA) can be formulated as:

$$\text{SpatMHSA}(z_q, x) = \sum_{t=1}^T \mathbf{W}_t \left[ \sum_{k=1}^K O_{tqk} \cdot \mathbf{W}_t' x_k \right], \quad (1)$$

where  $q \in \Omega_q$  denotes the query element with the representation feature  $z_q \in \mathbb{R}^D$ , and  $k \in \Omega_k$  indicates the key element with the representation feature  $x_k \in \mathbb{R}^D$ . Here,  $D$  denotes the feature dimension of  $z_q$  and  $x_k$ .  $\Omega_q$  and  $\Omega_k$  represent the set of query and key elements, respectively. The case where  $\Omega_q = \Omega_k$  is usually referred to as self-attention; otherwise, it is referred to as cross-attention. To disambiguate different spatial positions, the features  $z_q$  and  $x_k$  are the element-wise addition of the token and positional features in the implementation of our SpatMHSA.  $T$  denotes the total number of attention heads, and  $K$  represents the total number of key elements.  $\mathbf{W}_t \in \mathbb{R}^{D \times D_v}$  and  $\mathbf{W}_t' \in \mathbb{R}^{D_v \times D}$  denote the learnable projection weights, in which  $D_v = D/T$ . The notation of  $\cdot$  indicates the scalar multiplication operation.  $O_{tqk}$  represents the self-attention weights of the  $k$ -th sampling element in the  $t$ -th attention head. It is calculated by the scaled dot product between  $z_q$  and  $x_k$ , and is normalized over all key elements:

$$O_{tqk} \propto \exp \left( \frac{z_q^T \mathbf{U}_t^T \mathbf{V}_t x_k}{\sqrt{D_v}} \right), \quad \sum_{k=1}^K O_{tqk} = 1, \quad (2)$$

where  $\propto$  indicates the proportionality operation, and  $(\cdot)^T$  is the transpose operation.  $\mathbf{U}_t \in \mathbb{R}^{D_v \times D}$  and  $\mathbf{V}_t \in \mathbb{R}^{D_v \times D}$  are the learnable projection weights. Next, the output features of SpatMHSA are passed through an addition, normalization and feed forward network to yield the intermediate features.

After that, the intermediate features of each frame are fed into a temporal multi-head self-attention block, with the goal

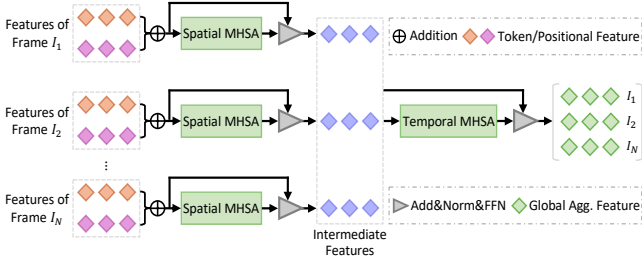


Figure 3: Illustration of the proposed STTM.

of effectively excavating long-range temporal dependencies across frames and performing inter-frame feature aggregation from a global perspective. Particularly, the calculation of the temporal multi-head self-attention (TempMHSA) can be represented by:

$$\begin{aligned} \text{TempMHSA}(z_q, \{x^n\}_{n=1}^N) \\ = \sum_{t=1}^T \mathbf{W}_t \left[ \sum_{n=1}^N \sum_{k=1}^K O_{tnqk} \cdot \mathbf{W}'_t x_k^n \right], \end{aligned} \quad (3)$$

where  $n$  indexes the input frame, and  $O_{tnqk}$  denotes the self-attention weights of the  $k$ -th sampling element in the  $t$ -th attention head and the  $n$ -th frame. The mathematical calculation of  $O_{tnqk}$  can be referred to as Equation (2), and it can be correspondingly normalized by  $\sum_{n=1}^N \sum_{k=1}^K O_{tnqk} = 1$ . The other symbols in Equation (3) have the same meanings as those in Equation (1). Finally, the output features of TempMHSA are sequentially fed into an addition and normalization operation, followed by a feed forward network to generate the global aggregated features.

### Spatial-Temporal GraphFormer Module

The illustration of the proposed STGM is depicted in Figure 4. Specifically, we first tokenize the frame feature  $f_n \in \mathbb{R}^{c \times h \times w}$  of the  $n$ -th frame into non-overlapping  $M$  ( $= h \times w$ ) token features with the dimension of  $D$ . Then, the token features and the corresponding positional features of each frame are added together and passed through a spatial GraphFormer block to explore short-range spatial dependencies within a frame and conduct intra-frame feature aggregation from a local perspective. Specifically, the spatial GraphFormer first constructs a fully-connected undirected graph  $\mathcal{G}(\mathcal{V}, \mathcal{E}, \mathbf{A})$ , in which  $\mathcal{V}$ ,  $\mathcal{E}$  and  $\mathbf{A} \in \mathbb{R}^{M \times M}$  respectively indicate the node set, edge set and adjacency matrix. In the construction of the graph, each input feature  $r_i \in \mathbb{R}^D$  (i.e., the addition of each token and positional features) is assumed to be a graph node  $v_i$ , and each edge  $e_{ij}$  is defined as the pairwise relationship between the nodes  $v_i$  and  $v_j$ . Particularly, the edge  $e_{ij}$  can be calculated as:

$$e_{ij} = \mathcal{F}_{map}(\Pi[Euc(r_i, r_j), Cos(r_i, r_j), Sec(r_i, r_j)]), \quad (4)$$

where  $\mathcal{F}_{map}(\cdot)$  denotes a mapping function consisting of two fully-connected layers, and  $\Pi[\cdot, \cdot, \cdot]$  represents the concatenation operation.  $Euc(\cdot, \cdot)$  means the standardized Euclidean distance, and  $Cos(\cdot, \cdot)$  denotes the cosine similarity.

$Sec(\cdot, \cdot)$  represents the semantic similarity, and  $Sec(r_i, r_j)$  can be calculated as  $r_i^T r_j$ . Based on the well-built edge  $e_{ij}$ , the adjacency matrix  $\mathbf{A}$  can be obtained through a softmax function, in which  $\mathbf{A}_{ij} = \exp(e_{ij}) / \sum_{j=1}^M \exp(e_{ij})$ .

Since the goal of our STGM is to perform feature aggregation from the local perspective of graph convolutions, directly utilizing a fully-connected graph cannot well model the local relationships between node features, in which case conducting graph convolutions may result in the aggregation of useless information (e.g., inter-class objects and backgrounds) and introduce much additional computational cost. To alleviate these problems, we present a graph pruning mechanism, with the goal of sparsifying the topological structure of the graph to attend the useful local relationships between nodes by removing useless/weak connection edges. Different from previous methods that employ a single cut-off threshold in the normalized adjacency matrix to remove edges, which may result in indistinguishable feature representations due to the elimination of matrix elements below the threshold, our customized graph pruning mechanism proposes to leverage  $S$  real-value thresholds denoted as  $\Gamma = [\theta_1, \theta_2, \dots, \theta_S]$ , in which  $\theta_i < \theta_j$  and  $\theta_i, \theta_j \in [0, 1]$  for  $\forall i < j$ . In light of this, we construct an adjacency tensor  $\mathbb{A} \in \mathbb{R}^{S \times M \times M}$  that consists of a set of adjacency matrices  $\{\mathbb{A}^s\}_{s=1}^S$ , where  $\mathbb{A}^s \in \mathbb{R}^{M \times M}$ . Particularly, we set  $\mathbb{A}^1$  as the identity matrix  $\mathbf{E}$ , and for each  $s \geq 2$ , the mathematical calculation of  $\mathbb{A}^s$  can be defined as:

$$\mathbb{A}_{ij}^s = \begin{cases} \mathbb{A}_{ij} & \text{if } \theta_{s-1} \leq \mathbf{P}_{ij} < \theta_s, i \neq j \\ 0 & \text{Otherwise} \end{cases}, \quad (5)$$

where  $\mathbf{P}_{ij}$  is an element in the probability matrix  $\mathbf{P}$  and it can be calculated by  $\mathbf{P}_{ij} = \lambda \cdot \mathbb{A}_{ij} / d_i$ , in which  $\lambda$  (is set as 0.3) denotes a scalar weight and  $d_i = \mathbf{D}_{ii} = \sum_{j=1}^M (\mathbf{A} + \mathbf{E})_{ij}$  is an element in the diagonal matrix  $\mathbf{D}$ . Next, building on the success of (Yun et al. 2019), we softly select two adjacency matrices  $\mathbf{Q}_1$  and  $\mathbf{Q}_2$  from the adjacency tensor  $\mathbb{A}$  via two  $1 \times 1$  convolutions with non-negative weights derived from the softmax function:

$$\mathbf{Q}_1 = \phi_1(\mathbb{A}, \text{softmax}(\mathbf{W}_{\phi_1})), \mathbf{Q}_2 = \phi_2(\mathbb{A}, \text{softmax}(\mathbf{W}_{\phi_2})), \quad (6)$$

where  $\phi_1(\cdot, \cdot)$  and  $\phi_2(\cdot, \cdot)$  denote two different  $1 \times 1$  convolution layers.  $\mathbf{W}_{\phi_1} \in \mathbb{R}^{1 \times 1 \times S}$  and  $\mathbf{W}_{\phi_2} \in \mathbb{R}^{1 \times 1 \times S}$  denote learnable parameters. Subsequently, the final pruned adjacency matrix  $\bar{\mathbf{A}} \in \mathbb{R}^{M \times M}$  can be calculated as:

$$\bar{\mathbf{A}} = \psi(\mathbf{Q}_1 \mathbf{Q}_2 + \mathbf{E}), \quad (7)$$

where  $\psi(\cdot)$  denotes the graph Laplacian normalization operation, which can be represented by  $\psi(\mathbf{Y}) = \mathbf{D}^{-\frac{1}{2}} \mathbf{Y} \mathbf{D}^{-\frac{1}{2}}$ . Empowered by Eqs. (5)-(7), we can obtain the pruned graph.

Based on the pruned graph, we extend the native graph convolutional network (Kipf and Welling 2017) from the static setting to the dynamic setting, and customize a dynamic graph convolution block with residual connections to effectively aggregate beneficial information from local neighbors. Particularly, the customized dynamic graph convolution block (DGCB) can be defined as:

$$\text{DGCB}(\mathbf{H}) = \text{DGCL}_2(\text{DGCL}_1(\mathbf{H})) + \rho \cdot \mathbf{H}, \quad (8)$$

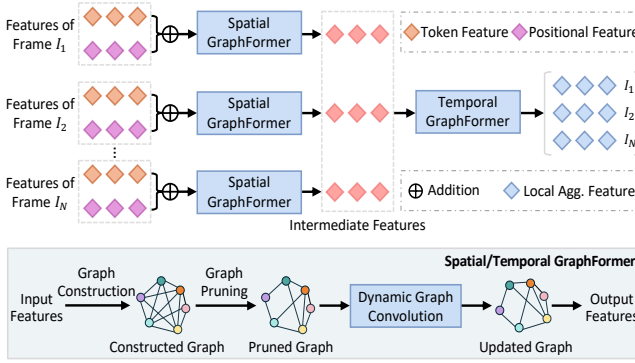


Figure 4: Illustration of the proposed STGM.

where  $\mathbf{H} \in \mathbb{R}^{D \times M}$  is the node feature matrix of the pruned graph.  $\text{DGCL}_1(\cdot)$  and  $\text{DGCL}_2(\cdot)$  denote two sequential dynamic graph convolution layers, which improve the native graph convolution calculation in (Kipf and Welling 2017). In detail, different from the graph convolution in (Kipf and Welling 2017) that uses a fixed adjacency matrix for all layers, our customized dynamic graph convolution re-calculates the adjacency matrices according to the newly learned node feature matrices at each layer, which facilitates capturing the dynamic graph structures during the graph convolution process and thus improves the effectiveness of the graph convolution.  $\rho$  denotes the residual constant, which is empirically set as 0.5. As illustrated in Figure 4, the outputs of the spatial GraphFormer are denoted as intermediate features.

After that, the intermediate features of each frame are passed through a temporal GraphFormer block to excavate short-range temporal dependencies across frames and perform inter-frame feature aggregation from a local perspective, generating the local aggregated features that are complementary to the outputs of STTM. The spatial GraphFormer and temporal GraphFormer share the same workflow, but their difference lies in the input features. Specifically, in the spatial GraphFormer, the input features are the element-wise addition of the token and positional features within a frame. In the temporal GraphFormer, the input features are the multi-frame intermediate features output by the spatial GraphFormer.

## Global-Local Feature Blender Module

Given the fact that there exist indeterminate knowledge discrepancies between transformer global features and GraphFormer local features, simply assembling (e.g., concatenating or adding) these features is ineffective for significant performance improvement. To this end, we customize a global-local feature blender module, with the blender weights dynamically balanced depending on the input transformer global features and GraphFormer local features. Compared to the simple ensemble of global and local features, our elaborately-customized global-local feature blender module tends to be more flexible and effective. In particular, the calculation of the global-local feature blender module can be

formulated by:

$$\mathbf{B} = \alpha_{GF} \otimes \mathbf{G} + \alpha_{LF} \otimes \mathbf{L}, \quad (9)$$

where  $\mathbf{B} \in \mathbb{R}^{D \times NM}$  stands for the blended feature matrix of  $N$  frames.  $\mathbf{G} \in \mathbb{R}^{D \times NM}$  and  $\mathbf{L} \in \mathbb{R}^{D \times NM}$  respectively represent the global aggregated feature matrix output by STTM and the local aggregated feature matrix output by STGM. The notation of  $\otimes$  denotes the element-wise multiplication operator.  $\alpha_{GF} \in \mathbb{R}^{D \times NM}$  and  $\alpha_{LF} \in \mathbb{R}^{D \times NM}$  represent the blender weights, which can be formulated by:

$$\alpha_{GF}, \alpha_{LF} = \text{softmax}(\mathbf{W}_\alpha \Pi[\mathbf{G}, \mathbf{L}]), \quad (10)$$

where  $\mathbf{W}_\alpha \in \mathbb{R}^{2D \times 2D}$  denotes the trainable parameters of one linear projection layer.  $\Pi[\cdot, \cdot]$  is the concatenation operation between features. With the help of the elaborately-customized global-local feature blender module, our TGB-Former is capable of boosting the collaborative representations from transformer and GraphFormer to facilitate video object detection.

## Experiments

### Dataset and Metric

For fair and convincing comparisons, we conduct experiments on the ImageNet VID dataset (Russakovsky et al. 2015). It spans 30 object classes, and contains 3,862 training and 555 validation videos. Following the same protocols in previous video object detection works (An et al. 2024; Qi, Yan, and Wang 2024; Cui 2023; He et al. 2022b), we evaluate our method on the validation set and adopt the mean average precision (mAP) at an Intersection-over-Union (IoU) threshold of 0.5 as the evaluation metric.

### Implementation Details

**Network Architecture:** We choose DETR (Carion et al. 2020) as the baseline detection network, and utilize ResNet-101 (He et al. 2016) as the backbone network for fair comparisons. Following the common implementation protocols in (Jiang et al. 2020; Deng et al. 2020; Cui et al. 2021; Zhu et al. 2017; Bertasius, Torresani, and Shi 2018), we adjust the total stride of the last stage (i.e., Conv5) in ResNet-101 from 32 to 16. Besides, we adopt Swin transformer (Liu et al. 2021) as the backbone network for better performance.

**TGBFormer:** We employ a sinusoidal positional encoding as in DETR (Carion et al. 2020) to yield positional features. The number of object queries per frame is set as 80 when utilizing the ResNet-101 backbone and 64 when using the Swin transformer backbone. The number of attention heads in the spatial and temporal transformer is set as 6 and the number of dynamic graph convolution layers in the spatial and temporal GraphFormer is set as 2. The real-value thresholds in our graph pruning mechanism are set as  $\Gamma = [0.1, 0.3, 1]$ . The residual constant in Equation (8) is set as 0.5.

**Training and Testing Details:** Following the common practice in previous video object detection methods (An et al. 2024; Qi et al. 2023b; Wu et al. 2019), we utilize both ImageNet DET and ImageNet VID datasets to train our TGB-Former, and resize each input frame to a shorter dimension of 600 pixels for fair comparisons. We train our TGBFormer

Method	Pub. & Year	Backbone	Base Detector	mAP (%)	Runtime (ms)
OGEM (Deng et al. 2019)	ICCV-2019	ResNet-101	R-FCN	79.3	112.0
TCENet (He et al. 2022b)	AAAI-2020	ResNet-101	R-FCN	80.3	125.0
MEGA (Chen et al. 2020)	CVPR-2020	ResNet-101	Faster R-CNN	82.9	114.5
HVRNet (Han et al. 2020b)	ECCV-2020	ResNet-101	Faster R-CNN	83.2	—
DSFNet (Lin et al. 2020)	ACM MM-2020	ResNet-101	Faster R-CNN	84.1	384.5
EBFA (Han et al. 2020a)	ACM MM-2020	ResNet-101	Faster R-CNN	84.8	—
MINet (Deng et al. 2021)	TIP-2021	ResNet-101	Faster R-CNN	80.2	133.0
TransVOD (He et al. 2021)	ACM MM-2021	ResNet-101	Deformable DETR	81.9	>341.1
MAMBA (Sun et al. 2021)	AAAI-2021	ResNet-101	Faster R-CNN	84.6	110.3
CSMN (Han et al. 2021)	IJCV-2021	ResNet-101	Faster R-CNN	85.2	909.1
EOVOD (Sun et al. 2022)	ECCV-2022	ResNet-101	Faster R-CNN	79.8	49.0
QueryProp (He et al. 2022a)	AAAI-2022	ResNet-101	Sparse R-CNN	82.3	37.3
TSFA (He et al. 2022b)	PR-2022	ResNet-101	Faster R-CNN	82.5	125.0
MSTF (Xu et al. 2022)	TCSVT-2022	ResNet-101	Faster R-CNN	83.3	105.7
CFANet (Han et al. 2022)	TCSVT-2022	ResNet-101	Faster R-CNN	85.0	884.2
GMLCN (Han and Yin 2023)	TMM-2023	ResNet-101	Faster R-CNN	78.6	39.6
TransVOD++ (Qianyu et al. 2023)	TPAMI-2023	ResNet-101	Deformable DETR	82.0	—
ClipVID (Deng, Chen, and Wu 2023)	ICCV-2023	ResNet-101	DETR	84.7	25.5
DGRNet (Qi et al. 2023a)	TIP-2023	ResNet-101	Faster R-CNN	85.0	91.7
CETR (An et al. 2024)	AAAI-2024	ResNet-101	DAB-DETR	79.6	42.9
CDANet (Qi, Yan, and Wang 2024)	TMM-2024	ResNet-101	Faster R-CNN	85.4	80.6
TGBFormer (ours)	—	ResNet-101	DETR	<b>86.5</b>	<b>24.3</b>
TransVOD Lite (Qianyu et al. 2023)	TPAMI-2023	Swin-B	Deformable DETR	90.1	67.1
TGBFormer (ours)	—	Swin-B	DETR	<b>90.3</b>	<b>49.7</b>

Table 1: Performance comparison with some state-of-the-art video object detection methods on the ImageNet VID dataset. ‘—’ denotes the corresponding results are not publicly available. The best results are highlighted in the bold font.

on 4 Nvidia Tesla A100 GPUs by using the AdamW optimizer. The whole training procedure lasts for 150K iterations, with a learning rate of  $10^{-4}$  for the first 110K iterations and  $10^{-5}$  for the last 40K iterations. Besides, we also employ the same data augmentation as the work of (Chen et al. 2020) to make the training procedure more effective. At the testing phase, TGBFormer takes consecutive  $N$  (which is set as 25 by default) frames as inputs and outputs the detection results of all input frames at one stroke.

### State-of-the-Art Comparison

We compare our TGBFormer with several existing video object detection methods, and summarize the results in Table 1. As illustrated in Table 1, we group the competing methods into two categories by their backbones. Since most video object detection methods are built on the backbone of the ResNet family, we first compare our TGBFormer with the other methods under the ResNet-101 backbone for fair comparisons. With the ResNet-101 backbone, our TGBFormer achieves 86.5% mAP at the runtime of 24.3 ms, 1.1% absolute mAP improvement and more than  $3.3\times$  faster over the leading method CDANet (Qi, Yan, and Wang 2024). This is because CDANet neglects the long-range temporal dependencies and employs a non-parallel frame-wise detection fashion, which yields incomprehensive feature aggregation and slows down the running speed. Compared with QueryProp (He et al. 2022a), GMLCN (Han and Yin 2023) and ClipVID (Deng, Chen, and Wu 2023), which are specifically optimized for efficient inference in real-world scenarios, our TGBFormer leads in both accuracy and runtime. This demonstrates that our TGBFormer is

more friendly for real-world scenarios. The accuracy of our TGBFormer derives from customizing transformers and dynamic graph convolutional networks to perform more comprehensive feature aggregation, which considers both long-range and short-range spatial-temporal information and thus makes detection more robust to the issues like blur or occlusion in videos. The efficiency of our TGBFormer comes from the parallel sequence-wise detection manner, which simultaneously detects objects on all input frames.

Since our method is backbone agnostic, we also report the results of our method using a more advanced backbone Swin transformer Base (Swin-B), in which case our TGBFormer obtains 90.3% mAP at runtime of 49.7 ms, which has a 0.2% mAP improvement and more than  $1.3\times$  faster over the competing method TransVOD Lite (Qianyu et al. 2023).

### Ablation Study

**Effectiveness of each component in TGBFormer:** To validate the effectiveness of each component in our TGBFormer, we conduct experiments to study how they contribute to the final accuracy, and the results are presented in Table 2.

Method (a) denotes the baseline detector DETR (Carion et al. 2020) using the ResNet-101 backbone, and it achieves 77.6% overall mAP.

Method (b) integrates the spatial-temporal transformer module into (a), which brings a clear overall mAP improvement (from 77.6% to 83.3%).

Method (c) incorporates a lite-version (i.e., without utilizing the graph pruning mechanism) of the spatial-temporal GraphFormer module into (a), which improves the overall mAP from 77.6% to 82.5%. The reason is that the

Method	(a)	(b)	(c)	(d)	(e)	(f)
Transformer		✓		✓	✓	✓
GraphFormer w/o GP			✓	✓	✓	✓
Global-Local Blender				✓	✓	✓
Graph Pruning (GP)					✓	✓
mAP (%) (overall)	77.6	83.3	82.5	83.1	85.4	<b>86.5</b> <sub>↑11.4</sub>
mAP (%) (slow)	85.5	88.1	87.0	87.9	90.7	<b>91.8</b> <sub>↑7.7</sub>
mAP (%) (medium)	75.6	81.7	80.6	81.2	84.4	<b>85.6</b> <sub>↑13.2</sub>
mAP (%) (fast)	56.7	66.9	65.4	66.5	70.6	<b>71.9</b> <sub>↑19.1</sub>

Table 2: Ablation studies on each component. ‘w/o’ is the abbreviation for ‘without’. ‘slow/medium/fast’ represents the objects with ‘slow/medium/fast’ motions. The best results are boldfaced.

elaborately-customized spatial-temporal GraphFormer module can effectively aggregate short-range spatial and temporal information to facilitate video object detection and thus improve detection accuracy.

Method (d) adds the graph pruning mechanism into (c) to attend the useful local relationships between nodes by removing useless/weak connection edges. It leads to an increase of 0.6% overall mAP against (c), indicating that the graph pruning mechanism is effective in our TGBFormer.

Method (e) adds the spatial-temporal transformer module into (d), and employs a vanilla concatenation operation to integrate the transformer global features and GraphFormer local features. It achieves 85.4% overall mAP, outperforming (d) by 2.3% overall mAP, which further demonstrates the effectiveness of the spatial-temporal transformer module.

Method (f) is the proposed TGBFormer, which introduces the global-local feature blender module into (e) to adaptively couple the transformer global features and GraphFormer local features. It achieves 86.5% overall mAP, with a 1.1% improvement over (e), which validates the effectiveness of the global-local feature blender module. Moreover, our TGBFormer significantly outperforms (b)-(e), indicating that all proposed components contribute to better accuracy.

**Analysis on the Number of Dynamic Graph Convolution Layers in STGM:** In the customized STGM, we leverage two successive dynamic graph convolution layers to implement the spatial and temporal GraphFormer, as shown in Figure 4 and Equation (8). To comprehensively analyze the influence of the number of dynamic graph convolution layers on detection accuracy, we conduct some ablation studies in Table 3. As shown in Table 3, the mAP improves consistently when the number of dynamic graph convolution layers  $L_{DGC}$  increases, and it tends to be optimal when the value of  $L_{DGC}$  is up to 2. However, when further enlarging  $L_{DGC}$  from 2 to 4, the mAP is decreased by 0.9% (from 86.5% mAP to 85.6% mAP). This is because deep-layer graph topological structures possibly bring several ambiguous or even mistaken connection edges, in which case conducting dynamic graph convolutions would result in the aggregation of inter-class feature information or background information and thus inevitably decrease accuracy.

**Influence of the Number of Inference Frames in TGB-**

# $L_{DGC}$	0	1	2*	3	4
mAP (%)	83.5	85.8	<b>86.5</b>	86.1	85.6

Table 3: Analysis on the number of dynamic graph convolution layers in STGM. The default parameter setting is represented by the symbol of \*. The best result is boldfaced.

# $N$	1	10	15	20	25*	30
mAP (%)	79.5	83.2	84.8	85.9	<b>86.5</b>	86.3
Runtime (ms)	50.9	40.5	33.6	27.9	24.3	<b>21.7</b>

Table 4: Influence of the number of inference frames. \* denotes the default setting. The best results are boldfaced.

**Former:** At the inference/testing stage, we input consecutive  $N$  inference frames into TGBFormer to simultaneously predict the detection results of  $N$  inference frames, and thus the number of inference frames  $N$  is an important parameter that affects the accuracy and runtime of TGBFormer. Table 4 illustrates the influence of the parameter  $N$ . The results demonstrate that enlarging the value of  $N$  leads to both accuracy improvements and runtime decreases, and the best accuracy is achieved when  $N$  is set as 25. Interestingly, we find that the accuracy slightly decreases when increasing the number of inference frames from 25 to 30, but the runtime is further improved thanks to the elaborately-customized sequence-wise detection paradigm. The reason is that feeding more inference frames into TGBFormer may hamper the learning of GraphFormer and prevent it from exploiting useful local information from long-range temporal contexts. To strike the trade-off between accuracy and runtime, we select 25 as the default value of  $N$ .

## Conclusion

In this paper, we propose a novel Transformer-GraphFormer Blender Network (TGBFormer) for video object detection, which provides a new perspective on feature aggregation by combining the advantages of transformers and graph convolutional networks. Our TGBFormer includes three key technical improvements against existing video object detection methods. First, we customize a spatial-temporal transformer module to aggregate global contextual information by utilizing the long-range feature dependencies, which contributes to constituting the global representations of objects. Second, we design a spatial-temporal GraphFormer module to perform feature aggregation from the perspective of graph convolutions, which facilitates generating new local representations of objects that are complementary to the transformer outputs. Third, we develop a global-local feature blender module to adaptively couple transformer-style global features and GraphFormer-style local features, which is beneficial to generate comprehensive feature representations. We conduct extensive experiments on the public ImageNet VID dataset, and the results show that our TGBFormer sets new state-of-the-art performance.

## Acknowledgments

This work was supported in part by the Natural Science Foundation of Shandong Province under Grant 322024038; and in part by the Low-altitude Flight Intelligent Service Support Shandong Engineering Research Center under Grant 412024014.

## References

An, S.; Park, S.; Kim, G.; Baek, J.; Lee, B.; and Kim, S. 2024. Context Enhanced Transformer for Single Image Object Detection in Video Data. In *Proc. AAAI Conf. Artif. Intell. (AAAI)*, 682–690.

Bertasius, G.; Torresani, L.; and Shi, J. 2018. Object Detection in Video with Spatiotemporal Sampling Networks. In *Proc. Eur. Conf. Comput. Vis. (ECCV)*, 331–346.

Carion, N.; Massa, F.; Synnaeve, G.; Usunier, N.; Kirillov, A.; and Zagoruyko, S. 2020. End-to-end object detection with transformers. In *Proc. Eur. Conf. Comput. Vis. (ECCV)*, 213–229.

Chen, X.; Pan, J.; Lu, J.; Fan, Z.; and Li, H. 2023. Hybrid cnn-transformer feature fusion for single image deraining. In *Proc. AAAI Conf. Artif. Intell. (AAAI)*, 378–386.

Chen, Y.; Cao, Y.; Hu, H.; and Wang, L. 2020. Memory enhanced global-local aggregation for video object detection. In *Proc. IEEE Conf. Comput. Vis. Pattern Recognit. (CVPR)*, 10337–10346.

Chitta, K.; Prakash, A.; Jaeger, B.; Yu, Z.; Renz, K.; and Geiger, A. 2023. TransFuser: Imitation With Transformer-Based Sensor Fusion for Autonomous Driving. *IEEE Trans. Pattern Anal. Mach. Intell.*, 45(11): 12878–12895.

Cui, Y. 2023. Feature Aggregated Queries for Transformer-Based Video Object Detectors. In *Proc. IEEE Conf. Comput. Vis. Pattern Recognit. (CVPR)*, 6365–6376.

Cui, Y.; Yan, L.; Cao, Z.; and Liu, D. 2021. TF-Blender: Temporal Feature Blender for Video Object Detection. In *Proc. IEEE Int. Conf. Comput. Vis. (ICCV)*, 8138–8147.

Deng, C.; Chen, D.; and Wu, Q. 2023. Identity-Consistent Aggregation for Video Object Detection. In *Proc. IEEE Int. Conf. Comput. Vis. (ICCV)*, 13434–13444.

Deng, H.; Hua, Y.; Song, T.; Zhang, Z.; Xue, Z.; Ma, R.; Robertson, N.; and Guan, H. 2019. Object guided external memory network for video object detection. In *Proc. IEEE Int. Conf. Comput. Vis. (ICCV)*, 6678–6687.

Deng, J.; Pan, Y.; Yao, T.; Zhou, W.; Li, H.; and Mei, T. 2020. Single shot video object detector. *IEEE Trans. Multimedia*, 23: 846–858.

Deng, J.; Pan, Y.; Yao, T.; Zhou, W.; Li, H.; and Mei, T. 2021. MINet: Meta-Learning Instance Identifiers for Video Object Detection. *IEEE Trans. Image Process.*, 30: 6879–6891.

Han, L.; Wang, P.; Yin, Z.; Wang, F.; and Li, H. 2020a. Exploiting better feature aggregation for video object detection. In *Proc. ACM Int. Conf. Multim. (ACM MM)*, 1469–1477.

Han, L.; Wang, P.; Yin, Z.; Wang, F.; and Li, H. 2021. Context and structure mining network for video object detection. *Int. J. Comput. Vis.*, 129: 2927–2946.

Han, L.; Wang, P.; Yin, Z.; Wang, F.; and Li, H. 2022. Class-aware Feature Aggregation Network for Video Object Detection. *IEEE Trans. Circuits Syst. Video Technol.*, 32(12): 8165–8178.

Han, L.; and Yin, Z. 2023. Global Memory and Local Continuity for Video Object Detection. *IEEE Trans. Multimedia*, 5: 3681–3693.

Han, M.; Wang, Y.; Chang, X.; and Qiao, Y. 2020b. Mining inter-video proposal relations for video object detection. In *Proc. Eur. Conf. Comput. Vis. (ECCV)*, 431–446.

He, F.; Gao, N.; Jia, J.; Zhao, X.; and Huang, K. 2022a. QueryProp: Object Query Propagation for High-Performance Video Object Detection. In *Proc. AAAI Conf. Artif. Intell. (AAAI)*, 2620–2627.

He, F.; Li, Q.; Zhao, X.; and Huang, K. 2022b. Temporal-adaptive sparse feature aggregation for video object detection. *Pattern Recognit.*, 127: 108587.

He, K.; Zhang, X.; Ren, S.; and Sun, J. 2016. Deep residual learning for image recognition. In *Proc. IEEE Conf. Comput. Vis. Pattern Recognit. (CVPR)*, 770–778.

He, L.; Zhou, Q.; Li, X.; Niu, L.; Cheng, G.; Li, X.; Liu, W.; Tong, Y.; Ma, L.; and Zhang, L. 2021. End-to-End Video Object Detection with Spatial-Temporal Transformers. In *Proc. ACM Int. Conf. Multimedia (ACM MM)*, 1507–1516.

He, X.; Wu, J.; Huang, Z.; Hu, Z.; Wang, J.; Sangiovanni-Vincentelli, A.; and Lv, C. 2024. Fear-Neuro-Inspired Reinforcement Learning for Safe Autonomous Driving. *IEEE Trans. Pattern Anal. Mach. Intell.*, 46(1): 267–279.

Jiang, Z.; Gao, P.; Guo, C.; Zhang, Q.; Xiang, S.; and Pan, C. 2019. Video object detection with locally-weighted deformable neighbors. In *Proc. AAAI Conf. Artif. Intell. (AAAI)*, 8529–8536.

Jiang, Z.; Liu, Y.; Yang, C.; Liu, J.; Zhang, Q.; Xiang, S.; and Pan, C. 2020. Learning where to focus for efficient video object detection. In *Proc. Eur. Conf. Comput. Vis. (ECCV)*, 18–34.

Kipf, T. N.; and Welling, M. 2017. Semi-supervised classification with graph convolutional networks. In *Proc. Int. Conf. Learn. Representations (ICLR)*, 565–578.

Li, D.; Zhang, Z.; Chen, X.; and Huang, K. 2019. A Richly Annotated Pedestrian Dataset for Person Retrieval in Real Surveillance Scenarios. *IEEE Trans. Image Process.*, 28(4): 1575–1590.

Lin, L.; Chen, H.; Zhang, H.; Liang, J.; Li, Y.; Shan, Y.; and Wang, H. 2020. Dual semantic fusion network for video object detection. In *Proc. ACM Int. Conf. Multimedia (ACM MM)*, 1855–1863.

Liu, C.; Wu, X.; and Jia, Y. 2016. A hierarchical video description for complex activity understanding. *Int. J. Comput. Vis.*, 118: 240–255.

Liu, J.; Shahroudy, A.; Perez, M.; Wang, G.; Duan, L.-Y.; and Kot, A. C. 2020. NTU RGB+D 120: A Large-Scale

Benchmark for 3D Human Activity Understanding. *IEEE Trans. Pattern Anal. Mach. Intell.*, 42(10): 2684–2701.

Liu, Z.; Lin, Y.; Cao, Y.; Hu, H.; Wei, Y.; Zhang, Z.; Lin, S.; and Guo, B. 2021. Swin Transformer: Hierarchical Vision Transformer Using Shifted Windows. In *Proc. IEEE Int. Conf. Comput. Vis. (ICCV)*, 10012–10022.

Peng, Z.; Guo, Z.; Huang, W.; Wang, Y.; Xie, L.; Jiao, J.; Tian, Q.; and Ye, Q. 2023. Conformer: Local Features Coupling Global Representations for Recognition and Detection. *IEEE Trans. Pattern Anal. Mach. Intell.*, 45(8): 9454–9468.

Qi, Q.; Hou, T.; Lu, Y.; Yan, Y.; and Wang, H. 2023a. DGR-Net: A Dual-Level Graph Relation Network for Video Object Detection. *IEEE Trans. Image Process.*, 32: 4128–4141.

Qi, Q.; Hou, T.; Yan, Y.; Lu, Y.; and Wang, H. 2023b. TC-Net: A Novel Triple-Cooperative Network for Video Object Detection. *IEEE Trans. Circuits Syst. Video Technol.*, 33(8): 3649–3662.

Qi, Q.; Yan, Y.; and Wang, H. 2024. Class-Aware Dual-Supervised Aggregation Network for Video Object Detection. *IEEE Trans. Multimedia*, 26: 2109–2123.

Qianyu, Z.; Li, X.; He, L.; Yang, Y.; Cheng, G.; Tong, Y.; Ma, L.; and Tao, D. 2023. TransVOD: End-to-End Video Object Detection With Spatial-Temporal Transformers. *IEEE Trans. Pattern Anal. Mach. Intell.*, 45(6): 7853–7869.

Russakovsky, O.; Deng, J.; Su, H.; Krause, J.; Satheesh, S.; Ma, S.; Huang, Z.; Karpathy, A.; Khosla, A.; Bernstein, M.; et al. 2015. Imagenet large scale visual recognition challenge. *Int. J. Comput. Vis.*, 115: 211–252.

Sun, G.; Hua, Y.; Hu, G.; and Robertson, N. 2021. MAMBA: Multi-level Aggregation via Memory Bank for Video Object Detection. In *Proc. AAAI Conf. Artif. Intell. (AAAI)*, 2620–2627.

Sun, G.; Hua, Y.; Hu, G.; and Robertson, N. 2022. Efficient one-stage video object detection by exploiting temporal consistency. In *Proc. Eur. Conf. Comput. Vis. (ECCV)*, 1–16.

Wang, H.; Tang, J.; Liu, X.; Guan, S.; Xie, R.; and Song, L. 2022. Ptseformer: Progressive temporal-spatial enhanced transformer towards video object detection. In *Proc. Eur. Conf. Comput. Vis. (ECCV)*, 732–747.

Wu, H.; Chen, Y.; Wang, N.; and Zhang, Z. 2019. Sequence level semantics aggregation for video object detection. In *Proc. IEEE Int. Conf. Comput. Vis. (ICCV)*, 9217–9225.

Xu, C.; Zhang, J.; Wang, M.; Tian, G.; and Liu, Y. 2022. Multi-level Spatial-temporal Feature Aggregation for Video Object Detection. *IEEE Trans. Circuits Syst. Video Technol.*, 32(11): 7809–7820.

Yoo, J.; Kim, T.; Lee, S.; Kim, S. H.; Lee, H.; and Kim, T. H. 2023. Enriched CNN-Transformer Feature Aggregation Networks for Super-Resolution. In *Proc. IEEE Win. Conf. App. Comput. Vis. (WACV)*, 4956–4965.

Yun, S.; Jeong, M.; Kim, R.; Kang, J.; and Kim, H. J. 2019. Graph Transformer Networks. In *Proc. Adv. Neural Inf. Process. Syst. (NeurIPS)*, 11983–11993.

Zhang, J.; Jia, X.; Hu, J.; and Tan, K. 2022. Moving Vehicle Detection for Remote Sensing Video Surveillance With Nonstationary Satellite Platform. *IEEE Trans. Pattern Anal. Mach. Intell.*, 44(9): 5185–5198.

Zhu, X.; Su, W.; Lu, L.; Li, B.; Wang, X.; and Dai, J. 2021. Deformable DETR: Deformable Transformers for End-to-End Object Detection. In *Proc. Int. Conf. Learn. Represent. (ICLR)*, 1–16.

Zhu, X.; Wang, Y.; Dai, J.; Yuan, L.; and Wei, Y. 2017. Flow-guided feature aggregation for video object detection. In *Proc. IEEE Int. Conf. Comput. Vis. (ICCV)*, 408–417.